*Jurnal Biologi Tropis*

Original Research Paper

# Optimizing Nutrient Dosage and Photoperiod for *Scenedesmus* sp. Cultivation: Growth and Protein Enhancement for Aquaculture

**Zakiyyah Nur Inayah[1]*, Dewi Ratih Riski Damayanti[2], Kharisma Orchida[3], Dian Nur Eva[1], Muhammad Bilal Afrizal Fajr[1], Adif Pratama[1], Aura Nuha Salsabila[1], Maryam Nur Afifah[1]**

[1]Aquaculture (Kediri City Campus), Faculty of Fisheries and Marine Science, University of Brawijaya, Kediri City, Indonesia;
[2]Agroecotechnology (Kediri City Campus), Faculty of Agricultural and Forestry Bio-industry, University of Brawijaya, Kediri City, Indonesia;
[3]Aquaculture Technology, Banyuwangi State Polytechnic, Banyuwangi. Indonesia

**Article History**
Received : November 14th, 2026
Revised : November 20th, 2026
Accepted : November 24th, 2026

*Corresponding Author:
**Zakiyyah Nur Inayah**, Aquaculture (Kediri City Campus), Faculty of Fisheries and Marine Science, University of Brawijaya, Kediri City, Indonesia;
Email: zakiyyahninayah@ub.ac.id

**Abstract:** Microalgae are essential live feeds in aquaculture; yet maximizing biomass and protein yield requires precise culture optimization. This study evaluated the interactive effects of Walne medium dosage (A0: 0, A1: 0.5, A2: 1.0, A3: 2.0 mL.L$^{-1}$) and photoperiod (B1: 24L:0D, B2: 12L:12D) on the growth kinetics, water quality, and soluble protein of an indigenous freshwater isolate, Scenedesmus sp. ZNI-UBK001, from Mojoroto fish ponds, Kediri City. Cultures were grown in 1000 mL Erlenmeyer flasks for 7 days (22–24°C, 3500–4500 Lux LED, continuous aeration) using a Completely Randomized Factorial Design (n=3). Two-Way ANOVA and Tukey's HSD test ($p < 0.05$) indicated that Walne dosage significantly affected growth kinetics and protein yield ($p < 0.001$). Treatment A3B2 (2.0 mL.L$^{-1}$ Walne, 12L:12D) produced the highest cell density (200,000 ± 26,458 cells.mL$^{-1}$), specific growth rate ($\mu$ = 0.427 ± 0.018 day$^{-1}$), shortest doubling time (DT = 1.625 ± 0.069 days), and peak soluble protein (459.85 ± 73.38 mg.L$^{-1}$), with stable water quality (22–25°C; pH 7.44–8.90). Halving illumination duration under 12L:12D offers an estimated 50% reduction in lighting energy demand without compromising productivity, providing a promising strategy for protein-rich *Scenedesmus* sp. Cultivation.

**Keywords:** Aquaculture; Live feed; Nutrient optimization; Photoperiod; Protein yield; *Scenedesmus* sp.; Walne Medium; Water quality.

## Introduction

The rapid expansion of global aquaculture is pivotal to modern food security, accounting for over half of human aquatic animal consumption (Tacon & Shumway, 2024). As wild fisheries reach maximum sustainable yields, commercial hatcheries must intensify production to meet escalating protein demands (Boyd et al., 2022). However, early larval survival and physiological robustness remain a major bottleneck due to underdeveloped digestive systems lacking functional enzymes (Ribeiro et al., 2022). Early larvae rely on exogenous live feeds rich in essential macronutrients, amino acids, and polyunsaturated fatty acids (Arenas-Pardo et al., 2024).

Live feeds serve as the primary biological bridge between abiotic nutrients and larval nutrition. Among the diverse organisms used as live feeds, microalgae represent the fundamental base of the aquatic trophic pyramid (Sarıtaş et al., 2024). Microalgae are single-celled photosynthetic microorganisms capable of converting inorganic carbon, solar or artificial light, and dissolved macronutrients into highly bioavailable bio-complexes

This article is licensed under a Creative Commons Attribution 4.0 International License.

© 2026s The Author(s). This article is open access

(Tounsi et al., 2023; Tapia-López et al., 2024). In hatcheries, microalgae fulfill dual operational functions: first, as direct live food for herbivorous larvae, rotifers (Brachionus spp.), and brine shrimp (Artemia spp.); and second, as indirect water purifiers ("green water technology") that stabilize water quality, shade larval rearing tanks to reduce stress, and modulate bacterial microbial communities through competitive exclusion and bioactive exudates secretion (Cheng et al., 2023).

Among various microalgal taxa, green microalgae of the class Chlorophyceae, specifically the genus Scenedesmus, are ideal live feed candidates due to their high photosynthetic efficiency and structural resilience (Mathimani et al., 2025). *Scenedesmus* species tolerate environmental stresses well, such as fluctuations in temperature, light, and pH (Júnior et al., 2025). Furthermore, their biomass boasts an exceptional biochemical profile containing 30–60% crude protein by dry cell weight, essential amino acids, structural carbohydrates, functional pigments, and vital polyunsaturated fatty acids (Khodadadianzaghmari et al., 2024; Uguz et al., 2025).

Despite these advantages, commercial hatcheries often struggle to maintain consistent biomass yield and nutritional quality during scale-up (Ugya et al., 2025). Microalgal metabolic pathways are highly dynamic and react directly to abiotic factors, including nutrient availability and lighting regimes (Venckus & Lastauskienė, 2026). Unoptimized culture conditions frequently cause premature culture crashes, photoinhibition, nutrient depletion, or unwanted metabolic shifts, such as excessive carbohydrate accumulation at the expense of protein synthesis (Ziganshina et al., 2023).

Macronutrient availability, particularly nitrogen (N) and phosphorus (P), directly dictates growth kinetics and protein synthesis in autotrophic cultures. Nitrogen is fundamental for synthesizing amino acids, proteins, nucleic acids, and photosynthetic pigments, while phosphorus forms the structural backbone of cellular membranes, nucleic acids, and energy-transfer compounds like ATP (Chhandama et al., 2023). Under nutrient limitation, microalgae arrest protein synthesis and redirect fixed carbon into lipids or carbohydrates, whereas balanced nutrient availability promotes rapid cell division and enzymatic protein accumulation (Zheng et al., 2025).

To ensure balanced nutrition in hatchery cultures, Walne medium is widely recognized as a complete formulation providing macronutrients ($NaNO_3$, $NaH_2PO_4$), trace metals, chelating agents (EDTA), buffering agents, and essential B-complex vitamins (Priyanka et al., 2020). However, determining the optimal dosage concentration (0.0–2.0 $mL \cdot L^{-1}$) is critical. Under-dosing leads to early nitrogen starvation and stunted growth, whereas over-dosing induces osmotic stress, ion toxicity, chemical light-shading, and unnecessary economic waste (Gupta et al., 2025).

Light energy drives photoautotrophic metabolism, where photon capture by thylakoid light-harvesting complexes powers electron transport and carbon fixation via the Calvin-Benson-Bassham cycle (Yang et al., 2023). Photoperiod duration significantly influences photosynthetic efficiency and circadian rhythmicity (Chen et al., 2026). Although continuous lighting (24L:0D) is often assumed to maximize carbon assimilation, prolonged photon exposure can saturate the photosynthetic apparatus, generating reactive oxygen species (ROS) that damage Photosystem II reaction centers and inhibit protein synthesis (Koletti et al., 2025).

Conversely, incorporating an alternating light–dark cycle (12L:12D) aligns culture conditions with natural circadian biology. During the dark phase, microalgae utilize dark respiration to repair damaged Photosystem II complexes, break down accumulated carbohydrates to synthesize structural and enzymatic proteins, and complete cell division (Suárez Quintana et al., 2025). Furthermore, switching from 24L:0D to 12L:12D lighting represents an estimated 50% reduction in daily illumination duration and associated electrical power demand, offering the potential to lower operational costs without sacrificing biological productivity.

In addition to culture parameters, the origin of the microalgal strain plays a crucial role in operational success. Unlike commercial

laboratory strains that may experience reduced environmental adaptability after prolonged subculturing, indigenous wild-type strains possess high competitive fitness and thermal tolerance (Júnior et al., 2025). In this study, an indigenous freshwater isolate, Scenedesmus sp. ZNI-UBK001, was isolated from tropical freshwater fish ponds in Mojoroto, Kediri City, East Java, Indonesia, providing a locally adapted strain suited to dynamic environmental fluctuations.

To maximize the production potential of *Scenedesmus* sp. ZNI-UBK001, this study aimed to investigate and optimize the combined effects of Walne medium dosage levels (A0 = 0 mL.L$^{-1}$, A1 = 0.5 mL.L$^{-1}$, A2 = 1.0 mL.L$^{-1}$, A3 = 2.0 mL.L$^{-1}$) and photoperiod regimes B1 = 24h light:0h dark, B2 = 12h light:12h dark) using a Completely Randomized Factorial Design (CRD Factorial). Cultivated under controlled LED irradiance (3500–4500 Lux) and ambient room temperatures (22–24°C), the cultures were evaluated across growth kinetics, water quality dynamics, and crude protein content (via Lowry assay) to establish a scalable, energy-efficient protocol for sustainable aquaculture live feed production.

## METHOD

### Microalgal Isolation and Strain Origin

The microalga *Scenedesmus* sp. ZNI-UBK001 was isolated from freshwater fish pond water in Mojoroto, Kediri City, East Java, Indonesia, and purified into a unialgal culture. Taxonomic identification was conducted via optical microscopy based on diagnostic morphological characteristics, including predominantly solitary (single-celled), non-motile, spherical to broadly ellipsoidal vegetative cells with smooth cell walls completely lacking spines or bristles. Intracellularly, the cells possessed a green, parietal cup-shaped chloroplast containing a single prominent pyrenoid, and distinct cytoplasmic vacuoles in mature cells. Because molecular characterization (e.g., 18S rRNA or ITS sequencing) has not yet been performed, the isolate is conservatively designated at the genus level as an indigenous wild-type strain (*Scenedesmus* sp. ZNI-UBK001) rather than a confirmed novel species.

### Equipment Preparation and Sterilization Protocol

All glassware, culture vessels, aeration tubes, and sampling accessories were sterilized using chlorine at a dosage of 60 ppm for 24 hours (followed by neutralization with sodium thiosulfate), thoroughly washed and rinsed with distilled water and oven-dried. Culture media water was subjected to a two-step sterilization process: initial chemical sterilization using chlorine at a dosage of 60 ppm for 24 hours (followed by neutralization with sodium thiosulfate), followed by physical thermal sterilization in an autoclave at 121 °C and 1 atm pressure for 30 minutes to guarantee complete biological sterility.

### Experimental Design and Cultivation Setup

Cultivation was carried out in 1000 mL Erlenmeyer over a 7-day cultivation period. Continuous aeration was provided 24 hours per day to facilitate gas exchange and prevent cell sedimentation. The experiment was arranged in a Completely Randomized Factorial Design (CRD Factorial) consisting of two factors with three replicates (n = 3):

Factor A (Walne Medium Dosage): A0 = 0 mL.L$^{-1}$ (Control), A1 = 0.5 mL.L$^{-1}$, A2 = 1.0 mL.L$^{-1}$, and A3 = 2.0 mL.L$^{-1}$

Factor B (Photoperiod Regime): B1 = 24h light:0h dark (Continuous light) and B2 = 12h light:12 h dark (Natural light-dark cycle).

All treatments were maintained in a climate-controlled room at ambient temperature (22–24 ∘C). Illumination was provided by artificial white LED lights calibrated at an intensity of 3500–4500 Lux.

### Growth Kinetics

Cell density (cells.mL$^{-1}$) was evaluated daily using an Improved Neubauer Haemocytometer under an optical microscope. Specific growth rate (μ, day$^{-1}$)) and doubling time (DT, days) were calculated during the exponential phase:

$$\mu\ (\text{day}^{-1}) = \frac{\ln(N_t) - \ln(N_0)}{t}$$

μ: Specific growth rate (day$^{-1}$)., Nt: Final cell density (cells.mL$^{-1}$), N0: Initial cell density (cells.mL$^{-1}$), t: time required to increase the concentration of N0 to Nt (day)

$$t_d\ (\text{day}) = \frac{\ln 2}{\mu}$$

$t_d$ : Doubling time (day), Ln 2 : Constant (0.6931), μ = Specific growth rate value (SGR) (day$^{-1}$)

### Water Quality Monitoring

Water quality parameters were measured at standard sampling intervals (Days 1, 3, 5, and 7). Temperature (℃): Measured using a calibrated mercury (Hg) glass thermometer. pH: Measured using a digital calibrated pH meter. Free $CO_2$ (mg.L$^{-1}$): Quantified via titrimetric analysis using 0.0454 N NaOH solution with phenolphthalein indicator. Nitrate ($NO_3$) & Phosphate ($PO_4$): Measured colorimetrically using Salifert high-precision test kits according to the manufacturer's protocol.

### Soluble Protein Quantification

Soluble protein concentration (mg.L$^{-1}$) was determined at Day 0 and Day 7 using the Lowry method (Lowry et al., 1951). For sampling, each culture flask was gently homogenized, and a 1.0 mL whole-culture aliquot was pipetted directly as a sample. One analytical measurement was performed for each biological replicate (n = 3 independent flasks per treatment). Each 1.0 mL sample aliquot was reacted with alkaline copper reagent and diluted Folin–Ciocalteu reagent at room temperature in the dark, alongside a 1.0 mL distilled water reagent blank. Absorbance was recorded at 660 nm using a spectrophotometer. A calibration curve was constructed using Bovine Serum Albumin (BSA) working standards across a concentration range of 0–200 mg.L$^{-1}$ (0, 40, 80, 120, 160, and 200 mg.L$^{-1}$). Sample protein concentrations were calculated by interpolating the 660 nm absorbance values into the linear regression equation derived from the BSA standard curve (y = ax + b).

### Statistical Analysis

Data normality was verified using the Shapiro-Wilk test (α = 0.05). Two-Way Analysis of Variance (ANOVA) for CRD Factorial evaluated main and interaction effects. Means were separated using Tukey's HSD post-hoc test ($p < 0.05$). Superscript letter notations (a, b, c, d) indicate statistically significant differences between treatments for final peak cell density (cells.L$^{-1}$) on Day 7.

## Results and Discussion

### Growth Performance and Cell Density Kinetics

The growth dynamics of *Scenedesmus* sp. ZNI-UBK001 over 7 days are detailed in Table 1 and illustrated in Figure 1. High nutrient treatments (A3) demonstrated significant exponential expansion, whereas controls (A0) stalled early due to nutrient depletion. Notations in Table 1 represent significant statistical differences for peak microalgal cell density on Day 7.

**Table 1.** Daily Cell Density (×104 cells.mL$^{-1}$) of *Scenedesmus* sp. ZNI-UBK001 (Mean ± SD)

| Treatment | Day 1 | Day 3 | Day 5 | Day 7 |
|---|---|---|---|---|
| A0B1 | 1.00 ± 0.00 | 1.67 ± 0.58 | 2.00 ± 1.00 | 1.67 ± 0.58 $^{a}$ |
| A1B1 | 1.00 ± 0.00 | 4.00 ± 3.46 | 6.33 ± 3.51 | 8.33 ± 4.04 $^{b}$ |
| A2B1 | 1.00 ± 0.00 | 5.00 ± 2.00 | 8.67 ± 3.06 | 12.67 ± 2.08 $^{c}$ |
| A3B1 | 1.00 ± 0.00 | 5.00 ± 1.00 | 14.33 ± 4.51 | 18.33 ± 2.08 $^{d}$ |
| A0B2 | 1.00 ± 0.00 | 2.33 ± 0.58 | 2.33 ± 1.53 | 2.00 ± 1.00 $^{a}$ |
| A1B2 | 1.00 ± 0.00 | 5.67 ± 0.58 | 9.33 ± 0.58 | 10.00 ± 1.73 $^{b}$ |
| A2B2 | 1.00 ± 0.00 | 4.67 ± 0.58 | 11.67 ± 2.08 | 11.00 ± 3.46 $^{bc}$ |
| A3B2 | 1.00 ± 0.00 | 3.33 ± 0.58 | 12.33 ± 3.51 | 20.00 ± 2.65 $^{d}$ |

Note: Different superscript letters indicate significant statistical differences ($p < 0.05$) specifically for final cell density on Day 7.

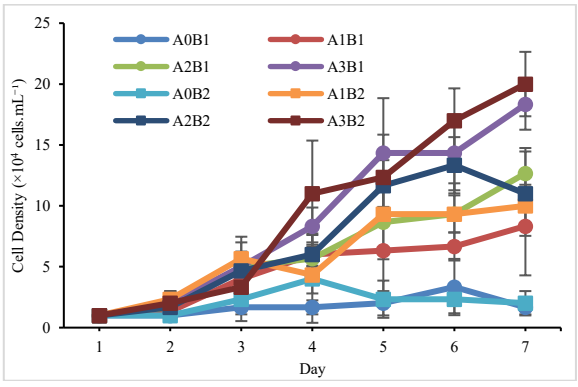


**Figure 1.** Cell Density Growth Curves Over 7 Days (×10$^4$cells.mL$^{-1}$)

### Specific Growth Rate (μ) and Doubling Time (DT )

Specific growth rates and doubling times calculated from cell density are presented in Table 2. Two-Way ANOVA demonstrated that Walne medium dosage exerted a highly significant main effect on both specific growth rate ($F = 12.38$, $p = 0.000$) and doubling time ($F = 6.29$, $p = 0.005$).

**Table 2.** Growth Kinetics and Specific Parameters of *Scenedesmus* sp. ZNI-UBK001 (Mean ± SD)

| Treatment | μ(day⁻¹) | DT(days) |
|---|---|---|
| A0B1 | 0.177 ± 0.106 [a] | 4.774 ± 2.124 [b] |
| A1B1 | 0.293 ± 0.064 [ab] | 2.236 ± 0.471 [ab] |
| A2B1 | 0.361± 0.023 [b] | 1.923 ± 0.119 [a] |
| A3B1 | 0.415 ± 0.017 [b] | 1.673 ± 0.069 [a] |
| A0B2 | 0.244 ± 0.106 [ab] | 3.155 ± 1.093[ab] |
| A1B2 | 0.327 ± 0.026 [ab] | 2.127 ± 0.179 [a] |
| A2B2 | 0.338 ± 0.042 [ab] | 2.069 ± 0.240 [a] |
| A3B2 | 0.427 ± 0.018 [b] | 1.625 ± 0.069 [a] |

In contrast, photoperiod regime showed a non-significant main effect on μ ($F = 0.83$, $p = 0.376$) and DT ($F = 1.71$, $p = 0.209$), and the interaction between Walne dosage and photoperiod was not statistically significant for μ ($F = 0.58$ , $p = 0.637$) and DT ($F = 0.69$, $p = 0,567$). Tukey's HSD post-hoc test ($p < 0.05$) confirmed that treatment A3B2 achieved the highest specific growth rate (0.427 ± 0.018 day⁻¹) and shortest doubling time (1.625 ± 0.069 days, which differed significantly from A0, A1, and A2 treatments ($p < 0.05$), though not significantly from A3B1 (0.415 ±0.017 day⁻¹ and 1.673 ± 0.069 days, respectively).

### Soluble Protein Accumulation

Soluble protein content determined by the Lowry method increased substantially with higher Walne medium dosages (Table 3, Figure 2). Two-Way ANOVA confirmed a highly significant main effect of nutrient dosage ($F=50.64$, $p<0.001$) as well as a statistically significant main effect of photoperiod regime ($F=5.24$, $p=0.036$). Conversely, the interaction effect between Walne dosage and photoperiod was not statistically significant. Post-hoc separation using Tukey's HSD test ($p < 0.05$) showed significant stepwise increases in final soluble protein across each nutrient dosage level, reaching a maximum of 459.85 ± 73.38 mg.L⁻¹ in treatment A3B2.

**Table 3.** Initial and Final Protein Content (mg.L⁻¹) across Treatments

| Dosage | Photoperiod | Initial Protein (mg.L⁻¹) | Final Protein (mg.L⁻¹) |
|---|---|---|---|
| A0 | B1 (24L:0D) | 31.07 ± 4.46 [a] | 54.97 ± 8.58 [a] |
| | B2 (12L:12D) | 31.79 ± 3.78 [a] | 67.79 ± 16.79 [a] |
| A1 | B1 (24L:0D) | 44.88 ± 3.93 [ab] | 135.49 ± 34.23 [ab] |
| | B2 (12L:12D) | 43.45 ± 9.10 [ab] | 165.74 ± 45.96 [ab] |
| A2 | B1 (24L:0D) | 63.45 ± 12.70 [ab] | 228.56 ± 20.00 [bc] |
| | B2 (12L:12D) | 54.88 ± 0.41 [ab] | 267.28 ± 43.07 [bc] |
| A3 | B1 (24L:0D) | 90.12 ± 23.11[b] | 351.90 ± 96.72 [cd] |
| | B2 (12L:12D) | 93.21 ± 45.81[b] | 459.85 ± 73.27 [d] |

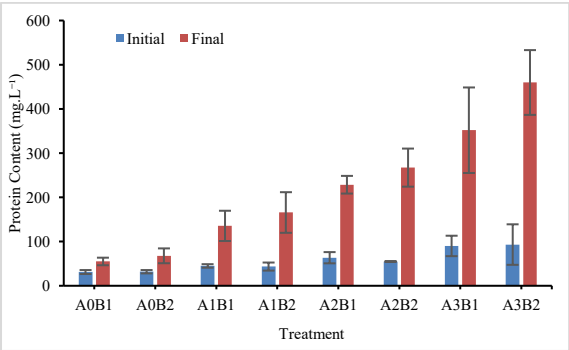


**Figure 2.** Comparison of Final Protein Content (mg.L⁻¹) Between B1 and B2 Regimes

### Water Quality Dynamics

Water quality parameters remained stable and within suitable ranges for Scenedesmus sp. cultivation throughout the 7-day experimental period under both photoperiod regimes (Table 4). Temperature, pH, nitrate ( $NO_3^-$ ), phosphate ($PO_4^{3-}$ ), and free $CO_2$ exhibited comparable ranges between continuous illumination (B1) and the 12L:12D photoperiod (B2), with slightly narrower pH and free $CO_2$ fluctuations observed under the B2 regime.

**Table 4.** Water Quality Parameters Across Treatments Over 7 Days (Range)

| Parameter | B1 | B2 | Optimal Range for *Scenedesmus* sp. |
|---|---|---|---|
| Temperature (°C) | 22.0 – 25.0 | 23.0 – 24.0 | 20.0 - 30.0 |
| pH | 7.46 – 8.90 | 7.44 – 8.60 | 6.80 – 8.80 |
| Nitrate ($NO_3$) (mg.L$^{-1}$) | 0.00 – 5.00 | 0.00 – 5.00 | 1.00 – 10.00 |
| Phospate ($PO_4$) (mg.L$^{-1}$) | 0.03 – 0.50 | 0.03 – 0.50 | 0.01 – 1.00 |
| Free $CO_2$ (mg.L$^{-1}$) | 3.99 – 9.99 | 3.99 – 7.99 | 2.00 – 12.00 |

## Discussion

### Physiological Mechanisms of Walne Medium Dosage on Growth Kinetics and Nitrogenous Metabolic Pathways

The empirical findings of this study provide clear, statistically supported evidence regarding the direct influence of Walne medium dosage levels on the growth kinetics, cell density, and protein accumulation of the wild-type freshwater isolate *Scenedesmus* sp. ZNI-UBK001. A stepwise, dose-dependent expansion in maximum cell density and soluble protein concentration was observed as Walne medium dosage increased from 0.0 ml.L$^{-1}$ (A0) to 2.0 ml.L$^{-1}$ (A3).

In autotrophic microalgal physiology, the rate of cell division and biochemical synthesis is governed by the availability of inorganic nitrogen and phosphorus (Venckus & Lastauskienė, 2026). Walne medium provides nitrogen primarily in the form of nitrate ( $NO_3^-$ ) and phosphorus as dihydrogen phosphate ( $H_2PO_4^-$ ), alongside essential trace elements chelating with EDTA (Priyanka et al., 2020). When *Scenedesmus* sp. ZNI-UBK001 cells absorb nitrate from the culture medium via active transport across the plasma membrane, the intracellular nitrate undergoes a two-step enzymatic reduction. First, cytosolic nitrate reductase (NR) reduces $NO_3^-$ to nitrite ( $NO_2^-$ ). Subsequently, chloroplastic nitrite reductase (NiR) reduces $NO_2^-$ to ammonium ($NH_4^+$) (Tapia-López et al., 2025).

The generated ammonium is rapidly incorporated into organic carbon skeletons via the Glutamine Synthetase - Glutamate Synthase (GS-GOGAT) pathway within chloroplasts (Nath et al., 2026). Glutamate and glutamine synthesized through this pathway serve as primary amino donors for transamination reactions catalyzed by aminotransferases, yielding essential amino acids including alanine, aspartate, serine, and glycine. These amino acids are subsequently polymerized at ribosome complexes to form structural, catalytic, and light-harvesting proteins (Li et al., 2018).

Under the A3 dosage regime (2.0 ml.L$^{-1}$ Walne medium), the elevated concentration of bioavailable nitrate maintained high intracellular pool levels of glutamine and glutamate, continuously driving protein translation (Gupta et al., 2025). This biochemical mechanism explains why treatment A3 achieved the highest crude protein yield (405.87 mg.L$^{-1}$ overall mean, peaking at 459.85±73.38 mg.L$^{-1}$ under A3B2). The colorimetric determination via the Lowry method—which specifically detects peptide bonds alongside aromatic amino acid residues (tyrosine and tryptophan) reacting with Folin-Ciocalteu reagent—directly reflects this accumulation of functional soluble proteins (Lowry et al., 1951).

Conversely, in the control treatments (A0=0.0 ml.L$^{-1}$ Walne medium), nitrogen availability was limited. Microalgae subjected to nitrogen depletion experience severe metabolic stress. As internal nitrogen reserves are depleted, nitrate reductase and GS-GOGAT activity drop sharply (Nath et al., 2026). To survive nitrogen starvation, microalgal cells activate autophagy and proteolysis, catabolizing intracellular structural proteins and light-harvesting phycobiliproteins or LHC complexes to recycle amino acids for essential survival functions (Tounsi et al., 2023). Furthermore, nitrogen deprivation triggers a metabolic re-routing of fixed carbon: fixed carbon from the Calvin cycle is diverted away from protein synthesis toward the pathway for triacylglycerol (TAG) or starch accumulation (Chhandama et al., 2023). As a result, A0 cultures ceased cell division early (20,000 cells.mL$^{-1}$ on Day 7), exhibited the lowest specific growth rates ($\mu$ = 0.177 – 0.244 day$^{-1}$), and minimal mean protein concentrations (61.38 mg.L$^{-1}$).

This pattern reveals an important insight into microalgal physiological adaptation: under nutrient-deficient conditions (A0), microalgal cells accumulate dense, heavy carbon storage compounds (lipids and carbohydrates/starch), maintaining cell weight despite minimal cell numbers (Yang et al., 2023). In contrast, under high

nutrient conditions (A3), cells undergo rapid, continuous mitotic divisions (200,000 cells.mL$^{-1}$), dividing into smaller, protein-dense daughter cells (autospores). Consequently, Walne nutrient supplementation enhances cellular protein quality and volumetric protein density rather than simply inflating physical dry cell mass.

**Photoperiod Energetics: Mitigating Photoinhibition and Optimizing Dark-Phase Respiration**

The experimental evaluation of photoperiod regimes demonstrated that the natural light-dark cycle (B2 = 12L:12D) consistently matched or outperformed continuous illumination (B1 = 24L:0D) across cell growth kinetics, doubling times, and protein yields. Specifically, treatment A3B2 achieved the maximum specific growth rate ($\mu = 0.427 \pm 0.018$ day$^{-1}$), the shortest doubling time (DT = 1.625 ± 0.069 days), and peak protein concentration (459.85 mg.L$^{-1}$).

Based on established photophysiological literature, this response can be interpreted through light-harvesting dynamics and photosynthetic energy conversion efficiency (Uguz et al., 2025). Autotrophic microalgal cells exposed to artificial light capture photons via chlorophyll a and b molecules in light-harvesting complexes. Prior studies suggest that under continuous illumination (24L:0D), prolonged photon pressure can exceed the capacity of electron transport chains and Calvin cycle carbon fixation, leading to excess excitation energy within the thylakoid membrane (Suárez Quintana et al., 2025). According to Koletti et al. (2025) and Li et al. (2022), such excess energy promotes triplet-state chlorophyll (3Chl*) formation and subsequent generation of reactive oxygen species (ROS)—including singlet oxygen ($^1O_2$), superoxide anions ($O_2^-$), and hydrogen peroxide ($H_2O_2$)—which can damage the D1 core protein of Photosystem II (PSII) and divert metabolic ATP toward antioxidant defense and protein repair rather than cell division (Cheng et al., 2023).

Conversely, incorporating a 12-hour dark period under the 12L:12D photoperiod (B2) is widely reported to alleviate continuous photo-oxidative stress, allowing cells to repair PSII complexes in the absence of photon pressure (Suárez Quintana et al., 2025). Furthermore, literature indicates that dark respiration enables microalgae to catabolize accumulated starch reserves via glycolysis and the tricarboxylic acid (TCA) cycle into carbon skeletons (alpha-ketoglutarate and oxaloacetate) and reducing equivalents (ATP and NADH), which serve as precursors for amino acid transamination and protein assembly (Nath et al., 2026; Zheng et al., 2025). From a cell-cycle standpoint, green microalgae such as *Scenedesmus* typically synchronize DNA replication, nuclear division, and autospore release during the dark phase (Sarıtaş et al., 2024). Although ROS levels, PSII quantum efficiency, and dark-phase enzymatic activities were not directly measured in this study, the consistently higher cell density (200,000 cells.mL$^{-1}$) and soluble protein yield (459.85- mg. L$^{-1}$) observed in A3B2 align closely with these documented circadian and photoprotective mechanisms.

Additionally, from an aquaculture engineering perspective, replacing continuous 24L:0D illumination with a 12L:12D photoperiod corresponds to an estimated 50% reduction in daily LED lighting duration and associated electrical power demand. While direct electricity consumption and operating expenses were not measured in this laboratory-scale study, halving the lighting schedule offers strong potential to reduce operational expenditures, heat load in indoor culture facilities, and carbon footprints, positioning A3B2 as an energy-conscious and scalable candidate protocol for commercial live feed production.

**Water Quality Dynamics, Carbon Balance, and Environmental Homeostasis**

Maintaining stable water quality conditions is essential for sustaining long-term microalgal cultures and preventing premature culture collapse (Ugya et al., 2025). Throughout the 7-day cultivation period, environmental parameters remained within optimal physiological ranges for *Scenedesmus* species (temperature: 22-25 °C; pH: 7.44-8.90). The temperature stability maintained by the controlled room climate (22-24 °C) provided an optimal thermal environment (Júnior et al., 2025). Temperatures within 22-25 °C support peak enzymatic activity for key metabolic enzymes-including Rubisco, nitrate reductase, and glutamine synthetase-without inducing thermal denaturation or membrane fluidity stress (Sanz-Luque et al., 2015).

The pH values across both photoperiod regimes fluctuated within a moderately alkaline

range (7.44–8.90 in B1 and 7.44–8.60 in B2), reflecting active photosynthetic carbon assimilation (Kalinina et al., 2023). As *Scenedesmus* sp. ZNI-UBK001 cells photosynthesize under LED light, they absorb dissolved free $CO_2$ and bicarbonate ions ($HCO_3^-$) from the culture medium via carbonic anhydrase enzymes. The removal of dissolved inorganic carbon shifts the carbonate-bicarbonate equilibrium:

$$HCO_3^- \leftrightarrow CO_2 + OH^-$$

The release of hydroxyl ions ($OH^-$) during bicarbonate uptake drives medium alkalization (Beltrán-Rocha et al., 2024). Notably, the upper pH limit remained slightly lower under the 12L:12D regime (8.60) than under continuous illumination (8.90), likely because respiratory $CO_2$ release during the 12-hour dark phase partially buffered photosynthetic alkalization. Overall, pH levels remained near the optimal range without requiring acid buffering.

Dissolved free $CO_2$ concentrations remained within stable, non-limiting ranges (3.99–9.99 mg.L$^{-1}$ in B1 and 3.99–7.99 mg.L$^{-1}$ in B2). Continuous 24-hour aeration, atmospheric gas diffusion at the air–water interface, and cellular dark respiration during the B2 dark phase continuously replenished dissolved inorganic carbon to support Calvin cycle carbon fixation (Yang et al., 2023).

Similarly, macronutrient concentrations spanned from initial enrichment levels down to depletion thresholds over the 7-day cycle (0.00–5.00 mg.L$^{-1}$ for nitrate and 0.03–0.50 mg.L$^{-1}$ for phosphate across both photoperiods). The reduction of nitrate toward 0.00 mg.L$^{-1}$ reflects active nitrogen assimilation into amino acids and soluble proteins, particularly in nutrient-supplemented cultures, whereas residual phosphate levels (0.03–0.50 mg.L$^{-1}$) remained within bioavailable limits to sustain ATP synthesis and phospholipid membrane integrity without inducing chemical precipitation (Chhandama et al., 2023).

## Conclusion

This study demonstrates that Walne medium dosage is the primary factor governing growth performance and protein synthesis in *Scenedesmus* sp. ZNI-UBK001, while photoperiod manipulation optimizes culture productivity. The A3B2 treatment combination (2.0 mL.L$^{-1}$ Walne medium dosage under 12L:12D photoperiod, 3500–4500 Lux LED, 22–24 °C, continuous aeration in 1000 mL Erlenmeyers) yielded the highest cell density (200,000 cells.mL$^{-1}$), specific growth rate ($\mu$=0.427 day$^{-1}$), shortest doubling time (1.625 days), and maximum soluble protein accumulation (459.85 mg.L$^{-1}$), alongside stable water quality conditions. Adopting a 12L:12D photoperiod offers an estimated 50% reduction in lighting duration and associated electrical energy demand without compromising biomass or protein yield, establishing a promising, resource-efficient protocol for protein-dense microalgal live feed production in sustainable aquaculture operations.

## Acknowledgement

The author expresses gratitude to the Directorate of Research and Community Service, Directorate General of Research and Development, Ministry of Higher Education, Science, and Technology, Indonesia (Direktorat Penelitian dan Pengabdian kepada Masyarakat Direktorat Jendral Riset dan Pembangunan Kementerian Pendidikan Tinggi, Sains dan Teknologi, Indonesia) for funding this research through the 2026 Bima Grant for Novice Lecturers (Hibah Penelitan Dosen Pemula Bima Tahun 2026). The authors also gratefully acknowledge Universitas Brawijaya and the Study Program Outside the Main Campus of Universitas Brawijaya in Kediri (PSDKU UB Kediri) for providing institutional support and laboratory facilities throughout this study.

## References

Arenas-Pardo, M. A., Gaxiola-Cortés, M. G., Barreto-Altamirano, A. F., Paredes-Medina, A. D. C., Palomino-Albarrán, I. G., Balam-Uc, P. M., Maldonado-Flores, J. C., & Álvarez-González, C. A. (2024). Changes in digestive enzyme activities during larval development of spotted seatrout (*Cynoscion nebulosus*). *Aquaculture Nutrition*, *2024*, 1309390. https://doi.org/10.1155/2024/1309390

Beltrán-Rocha, J. C., Guajardo-Barbosa, C., Barceló-Quintal, I. D., Reyna-Martínez, G., Fariz-Salinas, E., Ramírez-Castillo, A., Rodríguez-Fuentes, H., & López-Chuken, U. J. (2024). Effect of natural increase of

pH and microalgae cyclical re-cultivation on biomass production and polishing of municipal secondary effluent. *Desalination and Water Treatment*, *317*, 100103. https://doi.org/10.1016/j.dwt.2024.100103

Boyd, C. E., McNevin, A. A., & Davis, R. P. (2022). The contribution of fisheries and aquaculture to the global protein supply: Aquaculture and global protein. *Food security*, *14*(3), 805-827. https://doi.org/10.1007/s12571-021-01246-9

Cheng, P., Shan, S., Zhu, Z., Liu, K., Namsaraev, Z., Dubovskiy, I., & Xu, Q. (2023). The role of microalgae culture modes in aquaculture: a brief opinion. *Frontiers in Bioengineering and Biotechnology*, *11*, 1196948. https://doi.org/10.3389/fbioe.2023.1196948

Chhandama, M. V. L., Ruatpuia, J. V., Ao, S., Chetia, A. C., Satyan, K. B., & Rokhum, S. L. (2023). Microalgae as a sustainable feedstock for biodiesel and other production industries: Prospects and challenges. *Energy Nexus*, *12*, 100255. https://doi.org/10.1016/j.nexus.2023.100255

Gupta, S., Chelak, P., Das, M., Jha, M. K., & Das, A. (2025). Stress-induced enhancement of microalgal biochemical composition for sustainable biorefineries. *Discover Applied Sciences*, *7*(10), 1180. https://doi.org/10.1007/s42452-025-07545-6

Júnior, A. M. S., Faustino, S. M. M., e Holanda, F. H., Ferreira, I. M., & da Cunha, A. C. (2025). Kinetic parameters of *Scenedesmus obliquus* (Chlorophyceae) growth and yield under different cultivation conditions in vitro. *PeerJ*, *13*, e17879. https://doi.org/10.7717/peerj.17879

Kalinina, A., Naumov, V., Verakhina, A., Ovchinnikova, S., Yakovleva, D., Dobrov, A., Sokolava, T., Lukyanova, J., & Afanasieva, P. (2023). Study of the influence of the temperature and time of microalgae cultivation on the reproduction rate of *Chlorella* and *Scenedesmus* microalgae when cultured in a tubular photobioreactor. *Microbiology Research*, *14*(4), 2105-2112. https://doi.org/10.3390/microbiolres14040142

Khodadadianzaghmari, F., Jahadi, M., & Goli, M. (2024). Biochemical profile of *Scenedesmus* isolates, with a main focus on the fatty acid profile. *Food Science & Nutrition*, *12*(8), 5922-5931. https://doi.org/10.1002/fsn3.4254

Koletti, A., Skliros, D., Dervisi, I., Roussis, A., & Flemetakis, E. (2025). Oxidative stress responses in microalgae: modern insights into an old topic. Applied *Microbiology*, *5*(2), 37. https://doi.org/10.3390/applmicrobiol5020037

Li, J., Zhao, X., Chang, J. S., & Miao, X. (2022). A two-stage culture strategy for *Scenedesmus* sp. FSP3 for $CO_2$ fixation and the simultaneous production of lutein under light and salt stress. *Molecules*, *27*(21), 7497. https://doi.org/10.3390/molecules27217497

Li, S. Y., Ng, I. S., Chen, P. T., Chiang, C. J., & Chao, Y. P. (2018). Biorefining of protein waste for production of sustainable fuels and chemicals. *Biotechnology for Biofuels*, *11*(1), 256. https://doi.org/10.1186/s13068-018-1234-5

Lowry, O., Rosebrough, N., Farr, A. L., & Randall, R. (1951). Protein measurement with the Folin phenol reagent. *The Journal of Biological Chemistry*, 265-275.

Mathimani, T., Le, T. H. T., & Al-Ansari, M. M. (2025). Unraveling the bioenergy production potential of native Scenedesmus and *Nannochloropsis* species by ameliorating non-polar lipids and desirable fatty acid production. *Renewable Energy*, *238*, 122021. https://doi.org/10.1016/j.renene.2024.122021

Nath, A., Ahmad, A. S., Enkhbold, M., Elzhraa, F., & Kiskó, G. (2026). Process intensification for the protein production from microalgae: a comprehensive review. *Bioresources and Bioprocessing*, *13*(1), 126. https://doi.org/10.1186/s40643-026-01118-0

Priyanka, S., Kirubagaran, R., & Leema, J. M. (2020). Optimization of algal culture medium for zeaxanthin production by *Dunaliella tertiolecta*. *Current Science*, *119*(12), 1997-2005

Ribeiro, L., Hubert, F. N., Rodrigues, V., Rojas-Garcia, C., & Dinis, M. T. (2022). Understanding fish larvae's feeding biology to improve aquaculture feeding protocols. *Oceans*, *3*(1), 94-113. https://doi.org/10.3390/oceans3010009

Sanz-Luque, E., Chamizo-Ampudia, A., Llamas, A., Galvan, A., & Fernandez, E. (2015) Understanding nitrate assimilation and its regulation in microalgae. *Front. Plant Sci*, *6*, 899. https://doi.org/10.3389/fpls.2015.00899

Sarıtaş, S., Kalkan, A. E., Yılmaz, K., Gurdal, S., Göksan, T., Witkowska, A. M., Lombardo, M., & Karav, S. (2024). Biological and nutritional applications of microalgae. *Nutrients*, *17*(1), 93. https://doi.org/10.3390/nu17010093

Suárez Quintana, W. H., García-Rico, R. O., García-Martínez, J. B., Urbina-Suarez, N. A., López-Barrera, G. L., & Barajas-Solano, A. F. (2025). Effect of photoperiod duration and LED light quality on the metabolite profiles of high-mountain microalgal isolates. *Phycology*, *5(*4), 59. https://doi.org/10.3390/phycology5040059

Tacon, A. G., & Shumway, S. E. (2024). Critical need to increase aquatic food production and food supply from aquaculture and capture fisheries: trends and outlook. *Reviews in Fisheries Science & Aquaculture*, *32*(3), 389-395. https://doi.org/10.1080/23308249.2024.2324321

Tapia-López, L., Chairez-Oria, J. I., & Fernandez-Linares, L. C. (2025). Effect of nitrogen source and its concentration on *Scenedesmus dimorphus* productivity under photoautotrophic growth conditions. *Mexican Journal of Biotechnology*, *10*(3), 48-65. https://doi.org/10.29267/mxjb.2025.10.3.48-65

Tounsi, L., Ben Hlima, H., Hentati, F., Hentati, O., Derbel, H., Michaud, P., & Abdelkafi, S. (2023). Microalgae: a promising source of bioactive phycobiliproteins. *Marine Drugs*, *21*(8), 440. https://doi.org/10.3390/md21080440

Uguz, S., Sozcu, A., Simsek, E., & Yaslioglu, E. (2025). Nutritional and amino acid composition of *Scenedesmus* sp. cultivated under various light intensities. *Current Microbiology*, *82*(6), 274. https://doi.org/10.1007/s00284-025-04248-4

Ugya, A. Y., Chen, H., & Wang, Q. (2025). Enhancing the sustainability of microalgae cultivation through biosensing technology. *Materials Today Sustainability*, *31*, 101139. https://doi.org/10.1016/j.mtsust.2025.101139

Venckus, P., & Lastauskienė, E. (2026). Influence of light, temperature, and nutrient availability on growth and biochemical composition of *Scenedesmus quadricauda* cultivated in municipal wastewater. *Microorganisms*, *14*(1), 183. https://doi.org/10.3390/microorganisms14010183

Yang, Y., Zhao, J., Song, M., Yu, J., Yu, X., Ding, B., & Chen, X. (2023). Analysis of photosynthetic pigments pathway produced by CO2-toxicity-induced *Scenedesmus obliquus*. *Science of The Total Environment*, *867*, 161309. https://doi.org/10.1016/j.scitotenv.2022.161309

Zheng, J., Geng, J., Li, J., Li, D., Yang, S., Lu, X., Liu, J., Zhang, C., & Sun, H. (2025). Harnessing microalgae for protein production: advances, functional properties, and industrial potential. *Future Foods*, *12*, 100776. https://doi.org/10.1016/j.fufo.2025.100776

Ziganshina, E. E., Bulynina, S. S., Yureva, K. A., & Ziganshin, A. M. (2023). Optimization of photoautotrophic growth regimens of Scenedesmaceae alga: The influence of light conditions and carbon dioxide concentrations. *Applied Sciences*, *13*(23), 12753. https://doi.org/10.3390/app132312753